Available online at www.sciencedirect.com
ScienceDirect
Dyes and Pigments 75 (2007) 454–459
DYES and PIGMENTS
www.elsevier.com/locate/dyepig

Synthesis and properties of polymer containing azo-dye chromophores for nonlinear optical applications

Fengxian Qiu [a,*], Yonglin Cao [a], Hongliang Xu [a], Yan Jiang [a], Yuming Zhou [b], Juzheng Liu [b]

[a] School of Chemistry and Chemical Engineering, Jiangsu University, Zhenjiang 212013, PR China
[b] Department of Chemistry and Chemical Engineering, Southeast University, Nanjing 210096, PR China

Received 22 November 2005; received in revised form 23 March 2006; accepted 19 June 2006
Available online 12 September 2006

Abstract

Some thermal stable polyimides and polyimide/silica hybrid materials containing azo-dye have been synthesized. The resulting polyimides had high weight-average molecular weight (M_w) up to 49 300 and 53 900, respectively, and a large glass transition temperature (T_g) of 242 °C, and the decomposition temperature (T_d) of 350 °C. The resulting polyimide/silica hybrid materials had higher glass transition temperature and decomposition temperature than the pure polyimides. The silica content in the hybrid materials varied from 0 to 22.5 wt%. The electro-optic coefficients (γ_{33}) at the wavelength of 832 nm for polymer thin films poled were in the range of 9–23 pm/V and the values remained well (retained >83% for more than 100 h). The heat capacities of some materials were in the range of 0.8433–1.2564 J K^{-1} g^{-1} for the temperature range from 273 to 363 K. No thermal anomaly was found in this temperature range.

Keywords: Polyimide; Nonlinear optics; Electro-optical coefficient

1. Introduction

Polymeric nonlinear optical (NLO) materials have continuously drawn interest because they have several advantages for practical photonic applications of materials due to their excellent processability, and low dielectric constants [1,2]. Among the organic NLO molecules, azo-dye chromophores have been a special interest to many investigators because of their relatively large molecular hyperpolarizability (β) due to delocalization of the π-electronic clouds [3–5]. They were most frequently either incorporated as a guest in the polymeric matrix or grafted into the polymeric matrix. However, the ordered state of NLO active molecules obtained by the electric field poling process would normally decay to an equilibrium isotropic state due to thermal motion of the polymer chains [6,7]. Various approaches, including the incorporation of the chromophore into the polymer backbone (a main-chain or embedded side-chain system), an interpenetration polymer network method, and a cross-linking method, have been used to suppress the relaxation of NLO chromophores caused by the motion of polymer chains [8–10]. Because the latter methods tend to relatively lower glass transition temperature, the use of embedded side-chain polymers has been considered to be one of the best NLO matrix methods for stabilizing poled chromophores as well as retaining thermal stability of the polyimide backbone. However, most of the polymers have either low T_g or poor stability, which makes them unsuitable for direct use. To overcome these problems, one attractive approach is the incorporation of the organic nonlinear optical material into an inorganic matrix yielding an organic–inorganic hybrid material via sol–gel processing [11,12]. Recently, organic–inorganic hybrid nonlinear optical materials obtained through sol–gel process have received significant attention for their inherent properties of the silica matrix [13,14]. The hybrid

* Corresponding author. Tel.: +86 5112159861; fax: +86 5118617407.
E-mail address: fxqiuchem@163.com (F. Qiu).

0143-7208/$ - see front matter © 2006 Elsevier Ltd. All rights reserved.
doi:10.1016/j.dyepig.2006.06.037

materials offer the possibility of combining the advantages and overcoming the disadvantages of the two different materials. Sol–gel integrated optics has begun to show potential photomap applications and it stimulates studies on optical waveguide materials.

In this study, we synthesized two NLO chromophores containing azo-dye by changing the length in chemical structure (see Scheme 1), NLO polyimide (**PI-P-1**, **PI-P-2**) and polyimide/silica materials with different TEOS content (see Scheme 2). We reported here, detailed studies on the characterization of the polyimides and hybrids, as well as micrograph study, thermal and electro-optical properties.

2. Results and discussion

2.1. Characterization

Fig. 1, illustrates the FT-IR spectra of the prepared polyimide/silica hybrid materials **PH1-1**, **PH1-4**, **PH2-1** and **PH2-4**. The characteristic absorption bands of the imide groups were observed at 735, 1378, 1716, 1776 cm^{-1} for all samples as shown in Fig. 1 The absorption band around 1050–1150 cm^{-1} gradually increased intensity with increasing silica content, consistent with the formation of the three-dimensional Si–O–Si network in the hybrid film. The broad absorption bands around 3100–3300 cm^{-1} were assigned to the Si–OH reside, formed by the hydrolysis of alkoxy groups of TEOS. This band was barely detectable in the spectrum of **PH1-1** or **PH2-1** with lower silica content but increased its intensity in that of **PH1-4** or **PH2-4** with high silica content. Besides, the FT-IR spectrum consists of some peaks located at 1516 cm^{-1} (ν_{as}, –N=N–), whose intensity increased with chromophore **2**, 1364 cm^{-1} (ν_{str}, –C–N–C–), 1296 cm^{-1} (ν_s, $-NO_2$), 1452 cm^{-1} (N–H), 1378 cm^{-1} (wagging CH_2), 695 cm^{-1} (wagging N–H), 1727 cm^{-1} (ν_{as}, –C=O), indicating that the silica xerogel networks were composed of Si–O–Si backbones and some organic groups (CH_2–, NH–, OH). Figs. 2 and 3, show the SEM and TEM micrographs of the prepared polyimide/silica hybrid thin films **PH1-2** and **PH2-2**. In most cases, surface morphology of materials was of great importance for many technical applications requiring well-defined surfaces or interfaces. From Fig. 2, no phase separation could be observed. That is, covalent bonding (Si–O–Si) between the organic and inorganic components enhanced miscibility. They were homogeneously and uniformly dispersed at a molecular level. When the silica content was below 15 wt%, the silica particle size was 45 nm, which is shown in Fig. 3 These micrographs showed the fine interconnected or co-continuous phase morphology, which improved the efficiency of stress transfer mechanisms between the two components. Homogeneity was inferred by estimating the crystallinity of hybrids by powder XRD measurements. From Fig. 4, the diffraction patterns of **PH1-2** was found to

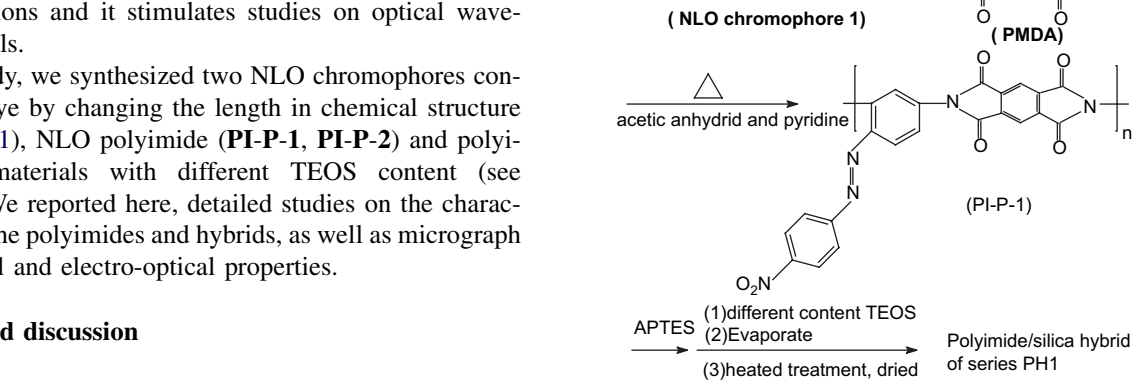

Scheme 2. Reaction scheme for preparing polyimide and polyimide/silica hybrid materials.

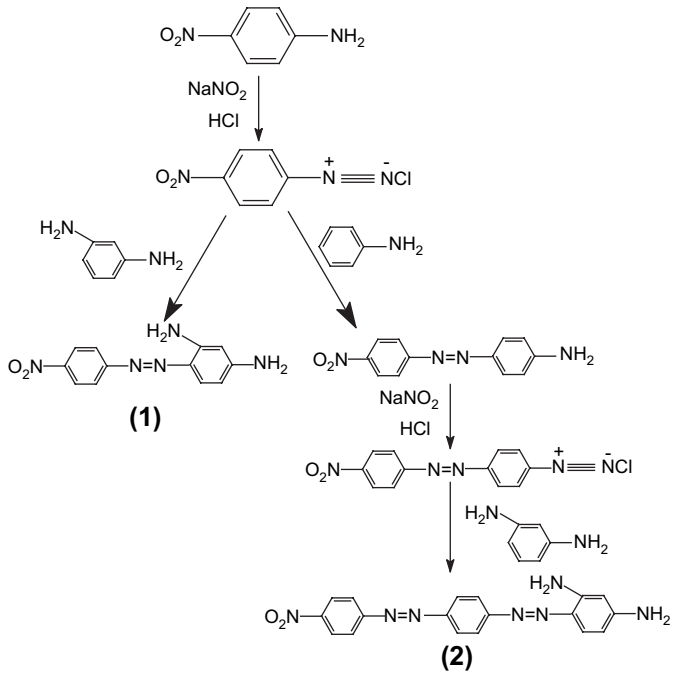

Scheme 1. Synthesis of chromophores **1** and **2**.

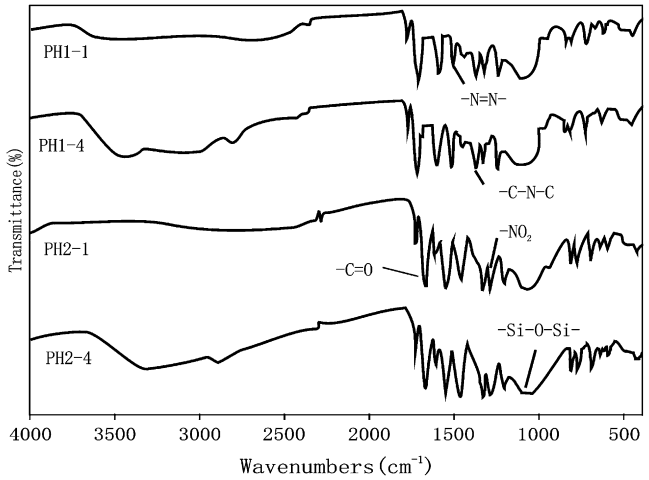

Fig. 1. FT-IR spectra of hybrid materials.

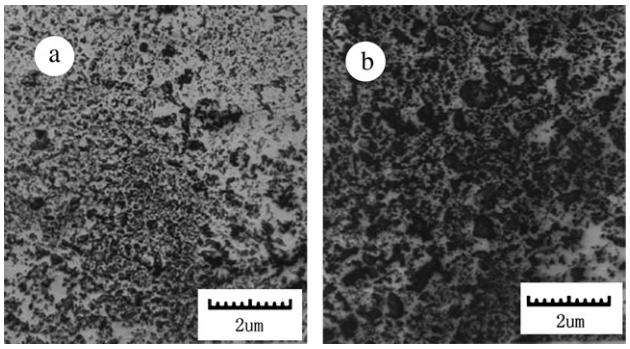

Fig. 2. SEM photographs of **PH1-2** (a) and **PH2-2** (b).

be featureless, showing only broad amorphous halos at $2\theta = 23.90°$, deriving from the homogeneous silica matrix. This result also indicated that covalent bonding (Si–O–Si) between the organic and inorganic components enhanced miscibility.

2.2. Thermal properties

To examine thermal activities of hybrid materials in higher temperature range and their thermal decomposition characteristics, DSC and TGA experiments were carried out on Netzsch STA449C with the heating rate 10 °C/min under nitrogen. Their data are listed in Table 1. The polyimide **PI-P-1** and series **PH1** are less thermally stable than the polyimide **PI-P-2** and series **PH2**. This is related to the differences in chromophore groups. It is therefore anticipated that the thermal stability of the NLO chromophore improves the stability of the final NLO polymer. The hybrid materials had higher glass transition temperature (T_g) than pure polyimide. Simultaneously, as in the table, the decomposition temperature (T_d) of hybrid materials increased with the increase of TEOS content. The enhanced thermal stability of hybrid materials was due to the formation of network of polyimide and the inorganic moieties, which resulted from the restriction of polymer chain mobility and became more intertwined with the rigid silica network. The T_d of azo-dye containing chromophore **2** system was higher than that of the azo-dye containing chromophore **1** system for the same TEOS content, because stability of the bisazochromophore was higher than that of the monoazomolecular

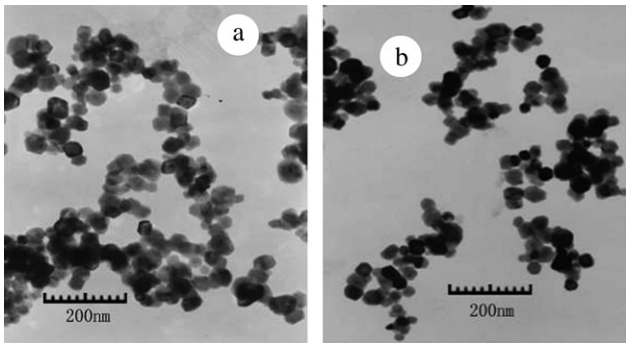

Fig. 3. TEM photographs of **PH1-2** (a) and **PH2-2** (b).

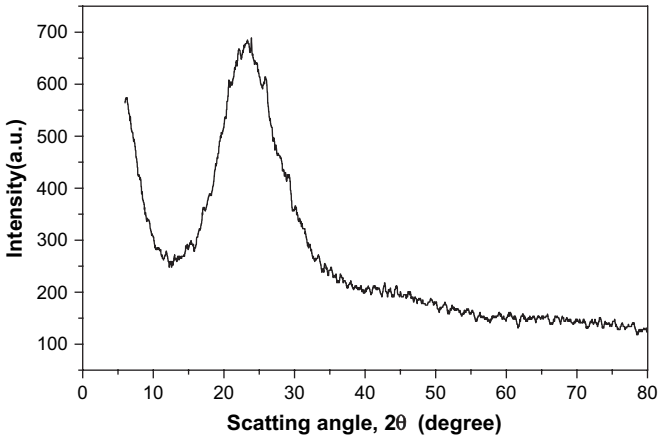

Fig. 4. XRD pattern of **PH1-2**.

chromophore. Therefore, the existence of covalent bonds between polyimide and silica impose even more restraint to chain movement in hybrids.

The heat capacity is a characteristic material property. Heat capacity values were measured with the Netzsch 204 F1, in nitrogen using Al, crucibles and lids. The measurement signal with the particular measuring heads must be corrected for any thermal asymmetries occurring with the increasing temperature. The baseline was obtained by running with empty crucibles or with crucibles containing a standard material (Sapphire) under the same measurement conditions used for the sample substance (atmosphere in the measuring cell, flow rate for operation with dynamic gas, initial temperature, heating rate and scanning rate (sampling interval), mass of crucible and lid and position of crucible in the cell). The Netzsch software performed the measurement setup and control, as well as the data acquisition of the temperature difference and absolute temperature. Therefore, we carried out all three measurements of a hybrid series in immediate succession on the same day. Several samples with the same test parameters could also be combined, with the same pair of measurements for the baseline and the standard. The entire temperature ranged over, which the C_p curve was to be

Table 1
Reactant summary and properties of hybrid systems

Hybrid materials	TEOS (wt%)	Diamine	T_g (°C)[a]	T_d (°C)[b]	γ_{33} (pm/V)	Appearance[c]
PI-P-1	0	1	242	350	16	
PH1-1	5	1	343	452	14	Transparent
PH1-2	10	1	348	466	13	Transparent
PH1-3	15	1	356	478	11	Transparent
PH1-4	22.5	1	378	482	9	Semi-transparent
PI-P-2	0	2	245	382	23	
PH2-1	5	2	352	465	22	Transparent
PH2-2	10	2	359	478	20	Transparent
PH2-3	15	2	366	482	18	Transparent
PH2-4	22.5	2	379	489	16	Semi-transparent

[a] Experimental results from DSC.
[b] Experimental results from TGA.
[c] UV–vis spectrum was observed.

determined, could be continuously scanned in a heating phase. Identical initial conditions must be guaranteed for the measurements of a series. The entire measuring system must be at a uniform, stable temperature level. To equalize the temperature in the system, a constant temperature segment prior to starting the heating phase (approximately 5 min) was defined.

After the run of three measurements (baseline, standard calibration material Sapphire as baseline + correction, sample also as baseline + correction), individual C_p values at different temperatures were determined according to the following equation:

$$C_p = \frac{m_{standard}}{m_{sample}} \times \frac{DSC_{sample} - DSC_{bas}}{DSC_{standard} - DSC_{bas}} \times C_{p,\ standard}$$

where:

C_p: heat capacity of the sample at temperature T, $J\,K^{-1}\,g^{-1}$
$C_{p,\ standard}$: heat capacity of the standard at temperature T, $J\,K^{-1}\,g^{-1}$
$m_{standard}$: mass of the standard, mg
m_{sample}: mass of the sample, mg
$DSC_{standard}$: value of DSC signal at temperature T from the standard curve, μV
DSC_{sample}: value of DSC signal at temperature T from the sample curve, μV
DSC_{bas}: value of DSC signal at temperature T from the baseline curve, μV.

The experiments were carried out to determine the heat capacities of the samples in the temperature range from 273 to 363 K. No thermal anomaly was found in this temperature range. The experimental data are listed in Table 2. From the table, it is inferred that the heat capacity tends to increase with the increase of the temperature. The heat capacity is one of the critical physical characters; the results would help us further investigate their other properties.

2.3. Electro-optical properties

High-quality films could be easily prepared from the polyimides and hybrid solutions in NMP by spin coating on indium-tin-oxide glass or other substrates. The electro-optic (EO) coefficient measurement of our nanohybrid was performed at a wavelength of 832 nm. The test sample consisted of a high-index prism, a thin silver film, a poled material layer, a buffer layer, and a base silver film. The silver film was thermally evaporated onto the hypotenuse face of a high-index prism as the first electrode. The thickness of the film was about 55 nm. A polymer was spin coated onto the silver substrate to a thickness of 1–2 μm, which can support four or five surface-plasmon modes with TE or TM polarization. A polymer buffer layer was then coated onto the polyimide film to a thickness of 3–5 μm or so. Corona discharge poling was performed by alignment of the chromophore dipoles in a high static electric field while the polyimide was heated to high mobility close to its glass transition temperature. The poling voltage was 1500 V. Finally, another silver film was deposited onto the buffer layer as the second electrode. The γ_{33} values are listed in Table 1.

From Table 1, the thermal stability of hybrid was found to be higher than the corresponding pure polyimide but the γ_{33} coefficients of hybrids were smaller than the corresponding polyimide. This was due to the fact that the content of chromophore is smaller than the pure polyimide. The γ_{33} of the azo-dye containing chromophore **2** system was higher than that of the azo-dye containing chromophore **1** system for the same TEOS content, this may be because dipole moment (μ) and hyperpolarizabilities (β) of bisazochromophore were higher than the monoazomolecular chromophore. Moreover, the EO coefficient can be further enhanced through modification of the NLO chromophore, increase of the NLO chromophore concentration and/or optimization of the poling process to achieve larger orientation degree of the chromophore dipole moments. The thermal alignment stability of these polyimides and hybrids was investigated by in situ EO coefficients

Table 2
Experimental data of heat capacities for polyimide/silica hybrid materials

T (K)	C_p ($J\,K^{-1}\,g^{-1}$)		T (K)	C_p ($J\,K^{-1}\,g^{-1}$)		T (K)	C_p ($J\,K^{-1}\,g^{-1}$)	
	PH1-2	**PH2-2**		**PH1-2**	**PH2-2**		**PH1-2**	**PH2-2**
273.15	0.8433	1.1189	275.15	0.8510	1.1233	277.15	0.8585	1.1276
279.15	0.8659	1.1318	281.15	0.8731	1.1359	283.15	0.8802	1.1400
285.15	0.8872	1.1440	287.15	0.8940	1.1479	289.15	0.9007	1.1518
291.15	0.9073	1.1556	293.15	0.9137	1.1593	295.15	0.9201	1.1630
297.15	0.9263	1.1666	299.15	0.9324	1.1701	301.15	0.9384	1.1736
303.1	0.9443	1.1770	305.15	0.9501	1.1804	307.15	0.9558	1.1837
309.15	0.9614	1.1869	311.15	0.9669	1.1901	313.15	0.9723	1.1933
315.15	0.9776	1.1964	317.15	0.9828	1.1994	319.15	0.9880	1.2024
321.15	0.9931	1.2054	323.15	0.9980	1.2083	325.15	1.0029	1.2112
327.15	1.0078	1.2139	329.15	1.0125	1.2168	331.15	1.0172	1.2195
333.15	1.0218	1.2222	335.15	1.0263	1.2249	337.15	1.0308	1.2275
339.15	1.0352	1.2301	341.15	1.0395	1.2327	343.15	1.0438	1.2352
345.15	1.0479	1.2377	347.15	1.0521	1.2401	349.15	1.0562	1.2425
351.15	1.0602	1.2449	353.15	1.0642	1.2473	355.15	1.0681	1.2496
357.15	1.0719	1.2519	359.15	1.0757	1.2542	361.15	1.0795	1.2564
362.15	1.0834	1.2588						

measured using sample holder. Fig. 5 shows the long-term stability of the EO coefficients of the polyimide **PI-P-1** and the value retained >88% for more than 100 h. The initial values of polyimide **PI-P-2**, **PH1-1**, **PH1-2**, **PH2-1** and **PH2-2** retained >91, >84, >83, >89, and >88%, respectively, after 100 h. Therefore, these results showed that these polymers might be useful in photonic device applications.

3. Experimental section

3.1. Materials and characterization

The pyromellitic dianhydride (PMDA) was obtained from Beijing chemistry agent plant. The 3-aminopropyltriethoxysilane, APTES, was purchased from Nanjing Shuguang chemical plant. *N*,*N*-Dimethylformamide (DMF) was distilled. Tetrahydrofuran (THF) was purified by distillation and other reagents were obtained commercially.

IR spectra of the prepared thin films were obtained on a KBr pellet using Nicolet Avatar 360 spectrometer. The optical characteristic of materials was measured in ultraviolet and visible range by means of spectrophotometer (Shimadzu UV-240). The fracture surfaces of hybrid thin films were examined on the Sirion scanning electron microscope (SEM). Hitachi H-600 transmission electron microscope (TEM) measured the particle sizes. X-ray diffraction (XRD) patterns of SiO_2 were obtained with a Cu Kα X-ray source and a step of 0.02 (2θ) and run from $2\theta = 6-80^\circ$ at room temperature. Measurements of the heat capacities were conducted on a Netzsch 204 F1 instrument with 6–10 mg samples at a heating rate of 5 K min^{-1} under nitrogen atmosphere. To study the thermal stability, thermogravimetric analysis (TGA) and differential scanning calorimetry (DSC) were performed on Netzsch STA449C.

3.2. Synthesis of chromophores

3.2.1. 4-(4′-Nitrophenyl-diazenyl) phenyl-1,3-diamine (*1*)

To *m*-phenylenediamine (0.1 mol) were added 1 mL concentrated hydrochloric acid and 10 mL water to make its salt solution. *p*-Nitroaniline (0.10 mol), 10 mL H_2O, and $NaNO_2$ (0.10 mol) were mixed to form a paste, which was poured into a mixture of crushed ice and 1.5 mL concentrated hydrochloric acid. The reaction was carried out for 0.5 h in an ice bath. The diazonium salt solution was added slowly into the solution of *m*-phenylenediamine salt during stirring and the mixture reacted for 1 h. After neutralizing with ammonia water for 0.5 h, the product was filtered and washed with water until it becomes neutral. The compound was purified on a silica gel column with the eluant acetone to afford 22.1 g (86%) of 4-(4′-nitrophenyl-diazenyl) phenyl-1,3-diamine (**1**). m.p. is 201–202 °C. ^{1}H NMR (300 MHz, CD_3COCD_3, ppm): 8.11 (s, ArH, 1H), 8.06 (s, ArH, 1H), 8.00 (s, ArH, 1H), 7.83 (s, ArH, 1H), 7.11 (s, ArH, 1H), 6.60 (s, ArH, 1H), 6.13 (s, ArH, 1H), 3.36 (s, $ArNH_2$, 4H). Anal. Calcd for $C_{12}H_{11}N_5O_2$: C, 56.03%; H, 4.28%; N, 27.24%. Found: C, 56.06%; H, 4.25%; N, 27.29%.

3.2.2. 4-(4′-Nitrophenyl-2-yl) phenyl-1,3-diamine (*2*)

First, 4-(4′-nitrophenyl-diazenyl) aniline was synthesized similar to **1**, and then its diazonium salt solution was added drop wise into the solution of *m*-phenylenediamine salt during stirring and the mixture was allowed to react for 1 h. After neutralizing with ammonia water for 0.5 h, the resulting solid was filtered and washed with water until it becomes neutral. After drying, it was purified on a silica gel column with the eluant acetone to afford 29.6 g (82%) of 4-(4′-nitrophenyl-2-yl) phenyl-1,3-diamine (**2**). m.p. is 208–210 °. ^{1}H NMR (300 MHz, CD_3COCD_3, ppm): 8.11 (s, ArH, 1H), 8.06 (s, ArH, 1H), 7.98 (s, ArH, 1H), 7.83 (s, ArH, 1H), 7.47 (d, ArH, 2H, $J = 8.7$ Hz), 7.35 (d, ArH, 2H, $J = 8.7$ Hz), 6.67 (s, ArH, 1H), 6.53 (s, ArH, 1H), 6.11 (s, ArH, 1H), 3.35 (s, $ArNH_2$, 4H). Anal. Calcd for $C_{18}H_{15}N_7O_2$: C, 59.83%; H, 4.16%; N, 27.15%. Found: C, 59.88%; H, 4.17%; N, 27.19%. The synthetic route is shown in Scheme 1.

3.3. Synthesis of NLO polyimides (*PI-P-1*, *PI-P-2*)

4-(4′-Nitrophenyl-diazenyl) phenyl-1,3-diamine (**1**) (1.0 mmol) was dissolved in 5 mL of DMF at room temperature, followed by the addition of pyromellitic dianhydride (PMDA, 0.5 mmol) at once. The solution was stirred at room temperature for 8 h under nitrogen. The mixture of acetic anhydride and pyridine (8 mL/4 mL, 2:1) was added to the solution at room temperature and this mixture was stirred for 6 h, and then heated to 90 ° under nitrogen for another 3 h. The polymer was precipiated into methanol and collected by filtration. The solid was further purified by dissolved in THF and reprecipitating in methanol. The resulting polyimide **PI-P-1** was collected and washed with methanol in a Soxhlet extractor for 20 h and dried at 60 °C under vacuum for 24 h. ^{1}H NMR (300 MHz, CD_3COCD_3, ppm): 8.19 (s, ArH, 2H, $J = 8.7$ Hz), 8.05 (d, ArH, 2H), 7.97 (d, ArH, 2H,), 7.36 (s, ArH, 1H), 7.22 (d, ArH, 1H), 7.06 (d, ArH, 1H). Anal. Calcd for $C_{22}H_9N_5O_6$: C, 60.14%; H, 2.05%; N, 15.95%. Found: C, 60.22%; H, 2.00%; N, 16.02%. Due to the good solubility of the polyimides in THF, the molecular weight can be measured by GPC.

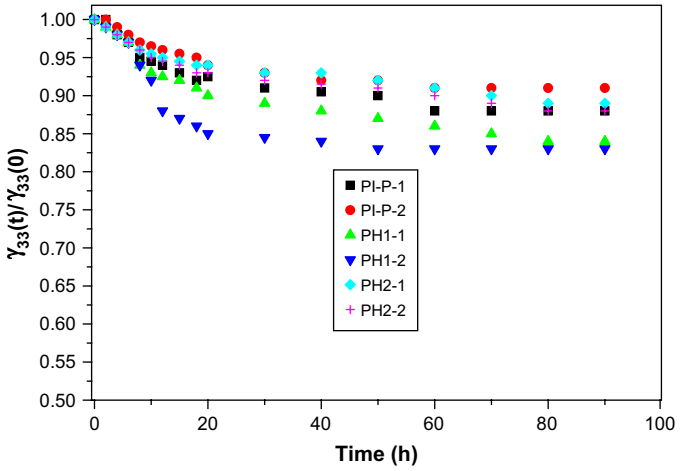

Fig. 5. Decay curve of EO coefficient of polarizing films.

The weight-average molecular weight (M_w) is 49 300 with a polydispersity of 2.33 (polystyrenes as standards).

Polyimide **PI-P-2** was synthesized by a procedure similar to that of polymer **PI-P-1** by using 4-(4′-nitrophenyl-2-yl) phenyl-1,3-diamine (**2**). ^{1}H NMR (300 MHz, CD_3COCD_3, ppm): 8.24 (s, ArH, 2H, $J = 8.7$ Hz), 8.07 (d, ArH, 2H), 8.02 (d, ArH, 2H), 7.88 (d, ArH, 2H, $J = 8.7$ Hz), 7.81 (d, ArH, 2H, $J = 8.7$ Hz), 7.46 (s, ArH, 1H), 7.35 (d, ArH, 1H), 7.19 (d, ArH, 1H). Anal. Calcd for $C_{28}H_{13}N_7O_6$: C, 61.88%; H, 2.39%; N, 18.05%. Found: C, 61.92%; H, 2.36%; N, 12.20%. The weight-average molecular weight (M_w) is 53 900 with a polydispersity of 2.37 (polystyrenes as standards).

*3.4. Preparation of polyimide/silica hybrid materials (series of **PH1**, **PH2**)*

Hybrid materials were synthesized via sol–gel process. The **PI-P-1** or **PI-P-2** solution was dissolved in DMF (15 mL) and stirred at room temperature for 3 h under nitrogen. Then, APTES, a coupling agent that provided the functional groups between the inorganic domains and the polymer matrix, was added. They were allowed to react for 4 h. At last, various content of TEOS were added as shown in Table 1. After 12 h of reaction, the homogeneous transparent sol could be obtained. Then the resulting homogeneous solution was transferred to a conical flask and was sealed by plastic film. After dried for 5 days and opened several small holes, the solvent evaporated slowly. The homogeneous transparent gel was formed. Then the sample was heated at 110 °C under vacuum for 2 h to remove residual solvent and by-products. The thermally stable hybrid materials were obtained. The synthetic route is shown in Scheme 2.

4. Conclusion

Two chromophores were synthesized with nitro-azobenzene structure. With these two chromophores, two series of nonlinear optical polyimides and polyimide/silica hybrid materials were also synthesized. They had network structure and silica particles were uniformly dispersed in the polymer matrix. The heat capacities of some samples were measured for the temperatures 273 and 363 K. The resulting NLO polyimides and polyimide/silica hybrids exhibited a relatively high T_g (>242 °C) and thermal stability up to 379 °C. Large EO coefficient values (9–23 pm/V) at the wavelength of 832 nm were achieved and the values remained well.

Acknowledgements

This work was financially supported by the Natural Science Foundation of Jiangsu Education (05KJB150016), the National Natural Science Foundation of China (50377005), and the Micro/Nano Science & Technology Fund of Jiangsu University (06JDG015).

References

[1] Burland DM, Miller RD, Walsh CA. Second-order nonlinearity in poled-polymer systems. Chem Rev 1994;94(1):31–75.
[2] Park KH, Lim JT, Song S, Lee YS, Lee CJ. Nonlinear optical polymers with novel benzoxazole chromophores. V. Linear and crosslinked polyurethanes using nitrothiophene and nitrophenol as electron acceptors. React Funct Polym 1999;40(2):177–84.
[3] Abbotto A, Beverina L, Chirico G, Facchetti A, Ferruti P, Pagani GA. Design and synthesis of new functional polymers for nonlinear optical applications. Synth Met 2003;139(3):629–32.
[4] Liu YG, Jiang AG, Xiang L, Gao J, Huang DY. Nonlinear optical chromophores with good transparency and high thermal stability. Dyes Pigments 2000;45(3):189–93.
[5] Luo JD, Qin JG, Kang H, Ye C. A postfunctionalization strategy to develop PVK-based nonlinear optical polymers with a high density of chromophores and improved processibility. Chem Mater 2001;13(3):927–31.
[6] Ghebremichael F, Kuzyk MG, Lackritz HS. Nonlinear optics and polymer physics. Prog Polym Sci 1997;22(6):1147–201.
[7] Yang SY, Peng ZH, Yu LP. Functionalized polyimides exhibiting large and stable second-order optical nonlinearity. Macromolecules 1994; 27(20):5858–62.
[8] Ranon PM, Shi YQ, Steier WH, Xu CZ, Wu B, Dalton LR. Efficient poling and thermal crosslinking of randomly bonded main-chain polymers for stable second-order nonlinearities. Appl Phys Lett 1993;62(21): 2605–7.
[9] Becker MW, Sapochak LS, Ghosen R, Xu CZ, Dalton LR, Shi YQ, et al. Large and stable nonlinear optical effects observed for a polyimide covalently incorporating a nonlinear optical chromophore. Chem Mater 1994;6(2): 104–6.
[10] Cui YJ, Wang MQ, Chen LJ, Qian GD. Synthesis and characterization of an alkoxysilane dye for nonlinear optical applications. Dyes Pigments 2005;65(1):61–6.
[11] Cornelius CJ, Marand E. Hybrid inorganic–organic materials based on a 6FDA–6FpDA–DABA polyimide and silica: physical characterization studies. Polymer 2002;43(8):2385–400.
[12] Hsu YG, Lin KH, Chiang IL. Organic–inorganic hybrid materials based on the incorporation of nanoparticles of polysilicic acid with organic polymers. 1. Properties of the hybrids prepared through the combination of hydroxyl-containing linear polyester and polysilicic acid. Mater Sci Eng B 2001;87(1):31–9.
[13] Sanchez C, Lebeau B, Chaput F, Boilot JP. Optical properties of functional hybrid organic–inorganic nanocomposites. Adv Mater 2003;15(23): 1969–94.
[14] Chaumel F, Jiang HW, Kakkar A. Sol–gel materials for second-order nonlinear optics. Chem Mater 2001;13(10):3389–95.